American Journal of Botany 93(11): 1588–1600. 2006.

BORDERED PIT STRUCTURE AND FUNCTION DETERMINE SPATIAL PATTERNS OF AIR-SEEDING THRESHOLDS IN XYLEM OF DOUGLAS-FIR (*PSEUDOTSUGA MENZIESII*; PINACEAE) TREES[1]

JEAN-CHRISTOPHE DOMEC,[2,4] BARBARA LACHENBRUCH,[2] AND FREDERICK C. MEINZER[3]

[2]Department of Wood Science and Engineering, Oregon State University, Corvallis, Oregon 97331 USA; and [3]USDA Forest Service, Forestry Sciences Laboratory, 3200 SW Jefferson Way, Corvallis, Oregon 97331 USA

The air-seeding hypothesis predicts that xylem embolism resistance is linked directly to bordered pit functioning. We tested this prediction in trunks, roots, and branches at different vertical and radial locations in young and old trees of *Pseudotsuga menziesii*. Dimensions of bordered pits were measured from light and scanning electron micrographs, and physiological data were from published values. Consistent with observations, calculations showed that earlywood tracheids were more resistant to embolism than latewood tracheids, mainly from earlywood having stretchier pit membranes that can distend and cover the pit aperture. Air seeding that occurs in earlywood appears to happen through gaps between the torus edge and pit border, as shown by the similar calculated pressures required to stretch the membrane over the pit aperture and to cause embolism. Although bordered pit functioning was correlated with tracheid hydraulic diameter, pit pore size and above all pit aperture constrained conductivity the most. From roots to branches and from the trunk base to higher on the trunk, hydraulic resistance of the earlywood pit membrane increased significantly because of a decrease in the size of the pit aperture and size and number of margo pores. Moreover, overall wood conductivity decreased, in part due to lower pit conductivity and a decrease in size and frequency of pits. Structural and functional constraints leading to the trade-off of efficiency against safety of water transport were also demonstrated at the individual pit level, with a positive correlation between pit membrane resistance on an area basis and the pressure differential required to cause membrane stretching, a characteristic that is essential for pit aspiration.

Key words: bordered pit; branch; earlywood; embolism; hydraulic architecture; latewood; margo; root; trunk.

The structure and physiological function of pit membranes in xylem conduits play important roles in tree hydraulic architecture by constraining where in the tree sap can flow at different water tensions. Understanding the linkages between key structural attributes and the function of pits provides insights on the effects of water tension on where water is available for replacing transpirational losses during photosynthetic gas exchange and on which of the xylem pathways are available for water movement. In spite of much research on the mechanism of pit function, there is little published work on the spatial patterns of pit function within a plant (Choat et al., 2005).

Embolisms within the xylem are thought to result from air seeding at pit membranes (Zimmermann, 1983; Crombie et al., 1985) rather than cavitation in the bulk phase of the liquid (Cochard et al., 1992). The cohesion–tension theory of water transport in plants explains the importance of a continuous water column (Zimmermann, 1983): if the water column is interrupted by an air bubble, the organ's specific conductivity declines. Increasingly low xylem pressures (Ψ_p) are, indeed, associated with a decrease in xylem conductivity (Jarbeau et al., 1995) as an increasing proportion of the conduits become embolized.

Both empirical and modeling studies show that under hydrated conditions the pit membrane in conifer tracheids is in a neutral position within the pit chamber, and water flows through the pores within the margo of the membrane. When the membrane is distended against the inside of the pit border, the torus usually blocks the aperture entirely (Liese and Bauch, 1967), thereby preventing water flow and the spread of embolism from embolized (gas-filled) tracheids to adjacent water-filled tracheids (Petty, 1972; Lancashire and Ennos, 2002; Hacke et al., 2004; Konrad and Roth-Nebelsick, 2005). However, the torus may not always cover the pit aperture entirely: a recent modeling effort showed that the slippage of the torus from its sealed position can create gaps large enough to allow embolism to develop in adjacent tracheids (Hacke et al., 2004). Therefore, it is currently unknown whether as a general rule air seeding actually occurs from an air bubble being pulled through pore openings, through ruptures in pit membranes when the margo is stretched beyond the point of rupture, or through membrane slippage that allows the torus to move off-center, exposing a portion of the margo in the pit aperture. The morphology of the pits will determine the water tension at which the tracheid becomes vulnerable to embolism. These pits (including both the borders and their membranes) may vary in morphology and frequency between species (Jansen et al., 2004), within species (Jutte and Spit, 1968), among organs (Shane et al., 2000), and between earlywood and latewood in the same growth ring (Kitin et al., 2004). Therefore, the spatial distribution of pit morphologies will affect the spatial distribution of vulnerability to embolism, which in turn will determine the effect of drought on water availability at different locations within the tree. The threshold pressure differential between two tracheids sharing one membrane at which an air bubble will be pulled through the membrane is inversely proportional to the size of the pit pores (the holes in the margo) (Zimmermann, 1983; Lewis, 1988).

[1] Manuscript received 14 December 2005; revision accepted 26 September 2006.

The authors wish to thank A. Soeldner for his help and advice on the SEM measurements. This work was supported by USDA CSREES NRI 97-35103-5052, USDA-CSREES NRI 03-35103-13713, and USDA Forest Service Ecosystem Processes Program (PNW 02-JV-1126952-252). They greatly appreciate the comments of two anonymous reviewers.

[4] Author for correspondence (e-mail: jc.domec@oregonstate.edu)

Other important morphological features include the depth of the pit, the diameter of the pit aperture and its location with respect to the location of the torus (if present) in the membrane, and the mechanical properties of the membrane itself, all of which will affect the extent to which the membrane can stretch before breaking and whether the torus will cover the aperture completely.

Because all water that ascends within the secondary xylem of conifers has to cross through bordered pits of overlapping tracheids, pit properties should be very important in controlling water movement. Thus, the frequency and properties of the pits will affect not only the mode of air seeding, but also the xylem's hydraulic conductance, implying that variation in the bordered pit structure could reflect the adaptive balance between hydraulic efficiency and hydraulic safety at different locations within a plant. The sizes of the openings between the margo strands are likely to be the hydraulic bottleneck controlling water flow between tracheids because water must move laterally through the membrane (Fujii et al., 2001), a requirement that explains the low radial xylem conductivity (Kitin et al., 2004; Domec et al., 2006). Therefore, in addition to conduit diameter, the size and frequency of the margo pores as well as overall pit frequency should be important anatomical determinants of tracheid hydraulic conductivity (Stone, 1939; McCully and Canny, 1988).

Little is known about within-tree differences in pit structure and function and their relationship to xylem hydraulic efficiency and safety in conifers. One useful tool for assessing hydraulic safety is the vulnerability curve (VC), which describes the relationship between the percentage of loss of hydraulic conductivity (caused by embolism) and Ψ_p. The pressure that reduces specific conductivity by 50% (P_{50}) can then be used to characterize xylem vulnerability to tension-induced embolism, and a number of studies have demonstrated that P_{50} is related to drought tolerance (Sperry and Tyree, 1990; Tyree et al., 1994; Maherali et al., 2004). Because Ψ_p is more negative at the top of the tree than anywhere else, we could expect the dimensions of the pit membrane pores to decrease and pit resistance to increase from the roots to the uppermost branches. The change in pit structure with height from roots to branches is currently unknown.

Vulnerability curves also suggest large differences in pit structure and function in the earlywood vs. the latewood within the same growth ring. In Douglas-fir, the earlywood has the typical sigmoidal curve, and it dominates in determining the shape of the curve for whole wood (earlywood plus latewood combined) (Domec and Gartner, 2002b). Latewood initially loses conductivity rapidly with decreasing Ψ_p in the water column, but then loses little additional conductivity with further decreases in Ψ_p. In latewood, the Ψ_p required to pull the meniscus through the largest pores in the membrane may be less negative than that needed to move the more rigid membrane, causing air-seeding to occur directly through the pores (Bolton and Petty, 1978). In earlywood, the porosity of the margo holding the torus is too large to prevent passage of the air meniscus at low Ψ_p, but the margo is elastic enough to allow the torus to be completely aspirated before air seeding can occur (Petty and Puritch, 1970). However, little is known about differences in the structural and mechanical properties of the pit membranes between earlywood and latewood of the same growth ring.

This paper is concerned with whether our current understanding of pit and membrane morphology and biomechanics explains the behavior of xylem hydraulic conductivity with changes in Ψ_p at different locations in Douglas-fir trees. We studied several bordered pit properties to determine whether conductivity and P_{50} are directly linked to the mechanical properties of the pit membrane. Specifically, we examined how the balance between hydraulic efficiency and safety of xylem is influenced by properties such as pit membrane pore size, membrane mechanical properties related to pressure differentials at which pit membranes are deflected, stretched, or ruptured; the hydraulic resistance of individual pits; and the contribution of pits vs. tracheid lumens to total xylem conductivity. Concurrent measurements on roots, trunks, and branches from old and young trees allowed a wide range of hydraulic and anatomical properties to be characterized.

MATERIALS AND METHODS

Hydraulic parameters—Hydraulic data described here were taken from published studies on Douglas-fir [*Pseudostuga menziesii* (Mirb.) Franco] trees growing in Oregon and Washington, USA. For roots, we used data from six 450-yr-old and six 23-yr-old trees from stands located within the Wind River Experimental Forest near the Wind River Canopy Crane Research Facility in southern Washington (Domec et al., 2004). Lateral medium roots 3–4 mm in diameter were excised near the base of the young and old trees at ~20 cm depth in the soil. For trunkwood and branches, we used data from six 110-yr-old and six 10-yr-old trees from the Cascade Range, Oregon (Domec and Gartner, 2001, 2002a). Four locations were sampled along the trunk of the old trees at nodes 5, 15, 35, and base (node 110) counting down from the top of the tree (Table 1). The term node is used in the forestry sense to signify the location of a whorl of branches. We sampled just distal to the nodes specified. At all the heights in the trunk but at the top of the trees, two radial locations were measured: the inner sapwood and the outer sapwood. In addition, a branch was sampled from nodes 5, 15, and 35 in three other trees from the same site. One trunk location and one branch, both taken at node 5, were sampled within the young trees.

The pressure required to cause a 50% loss of hydraulic conductivity from embolism (P_{50}) was derived from the vulnerability curves and used as a hydraulic parameter to be compared with the structure and function of bordered pits. All xylem vulnerability curves were determined using the air-injection method (Cochard et al., 1992). By including trunkwood samples from young and old trees and from roots and branches, we were able to obtain a wide range of P_{50} from a minimum of 1.0 MPa in roots to a maximum of 6.3 MPa in branches (Table 1).

We used root, trunk, and branch xylem pressures (Ψ_p) that represented the average minimum values of published data measured on the same trees and at the same root, trunk, and branch locations used to determine P_{50} (Domec and Gartner, 2002a; Domec et al., 2004) (Table 1). Briefly, trunk Ψ_p at the base of the trees was estimated using temperature-corrected stem psychrometers (Dixon and Tyree, 1984). Trunk Ψ_p in the upper crown was estimated using the bagged-leaf technique (Begg and Turner, 1970). Root Ψ_p was estimated by measuring the percentage loss of conductivity in roots collected from the field, then referring to previously determined vulnerability curves to calculate the corresponding values of Ψ_p in roots (Domec et al., 2004).

Light microscope observations of tracheid and bordered pit structures—We described tracheid and pit anatomy using the wood samples from the same trees as those used to determine P_{50}. For tracheid features, we measured the earlywood and latewood separately. For pit features, we used only earlywood to explain the behavior of whole wood because vulnerability to embolism in whole wood is dominated by the vulnerability to embolism of earlywood (Domec and Gartner, 2002b).

Using a sliding microtome, we cut permanent transverse, radial-longitudinal, and tangential-longitudinal sections from each sample used for vulnerability curves. Following a dehydration series, sections were stained with safranin O. Each section was analyzed with an image analysis system consisting of a compound microscope, video camera (MetaVue Imaging System, Universal Imaging Corp., Downingtown, Pennsylvania, USA), and the software NIH Image (Rasband, 1996).

For tracheid diameter (d_c), we measured on average 150 tracheids per growth ring per sample on transverse sections (30 μm thick) as follows. For

TABLE 1. Mean values of xylem pressure causing 50% loss of conductivity (P_{50}), minimum in situ xylem pressures (Ψ_p), whole-wood specific conductivity (k_s), bordered-pit specific conductivity on a tissue basis ($k_{s\text{-pit}}$), and the percentage of the total xylem resistivity (the inverse of k_s) represented by pits ($k_s/k_{s\text{-pit}}$) at different axial locations along the Douglas-fir (*Pseudotsuga menziesii*) trees sampled. The node numbers represent the height location in the trunk counting nodes down from the top of the trees. Values at each node in the trunk of the old trees represent the weighted average between outer and inner sapwood samples.

Tree location	Height (m)	P_{50} (MPa)	Ψ_p (MPa)	k_s ($kg \cdot m^{-1} \cdot s^{-1}MPa^{-1}$)	$k_{s\text{-pit}}$ ($kg \cdot m^{-1} \cdot s^{-1}MPa^{-1}$)	$k_s/k_{s\text{-pit}}$ (%)
Root, old	−0.2	−1.0	−0.7	4.2	6.4	66
Root, young	−0.2	−1.4	−1.5	3.6	5.2	69
Trunk base (node 110)	0.33	−3.3	−1.5	4.1	5.6	73
Trunk node 35	35	−3.3	−1.9	3.4	4.2	81
Trunk node 15	39	−3.6	−2.1	3.3	4.8	69
Trunk node 5	42	−4.7	−2.3	1.8	2.4	75
Trunk, young	5.6	−3.1	−1.6	1.9	2.2	86
Branch 5	42	−5.9	−2.6	1.0	1.9	53
Branch 15	39	−5.9	−2.3	0.9	1.7	53
Branch 35	35	−5.8	−2.0	0.7	1.1	64
Branch, young	5.6	−6.3	−2.5	0.6	0.8	75

each growth ring, we chose six radial files in which we measured all the tracheids from the growth ring boundary outward. We estimated the hydraulic mean conduit diameter D_c as $\Sigma d_c^5/\Sigma d_c^4$, which represents the diameter of the conduits that embolize at P_{50} (Kolb and Sperry, 1999). Our preliminary analyses showed that by ignoring latewood tracheids in the determination of D_c, we would have overestimated D_c by <4% in all of the samples. We then used the radial-longitudinal sections to find tracheids of approximate diameter D_c (±5% of the mean). Most of the tracheids in this diameter range were in the inner third of the earlywood, and for these tracheids we estimated bordered pit diameter (D_b) and pit aperture diameter (D_a) on 100–120 bordered pits per sample. The total bordered pits per cell wall area (pit frequency) were counted over the entire radial walls of the tracheids that also fell in the D_c range in each of the growth rings, for an average of 400–600 pits counted per sample. The surface represented by pits as a percentage of the radial cell wall area was then estimated by pit frequency times average pit area (from D_b), all divided by the ratio of the lumen area to the total area (lumen plus cell wall). We then estimated latewood values of D_b and D_a by measuring these values in the middle of the latewood of each of the 4–8 growth rings on each of these radial sections for a total of 45–60 measurements per sample. We used the thickness of the pit chamber as a surrogate for twice the maximum torus displacement (d_{max}), as measured on the tangential-longitudinal sections.

Membrane structure—We measured the fine bordered pit structures using a scanning electron microscope (SEM). We made a flat surface on the specimens with a razor blade or a microtome (Jansen et al., 1998). We then used critical point drying to lower the capillary tensions, thereby avoiding the potential drying artifacts, such as alteration of the ultrastructure of the membrane or increasing the incidence of aspirated pits (Thomas and Nicholas, 1966), that could be caused by regular drying of unaspirated pits (Exley et al., 1973). Wood specimens were then coated with a very thin layer of gold using a sputter coater to make the surface conductive. The samples were then imaged at magnifications ranging from 3000× to 8000× to observe earlywood and latewood pit structures, respectively.

Because of the difficulty of finding pits with both the torus and the margo strands when using the SEM, we aimed to take only seven images per growth ring (four in the earlywood and three in the latewood) for each of the several growth rings in the sample, for an average of 30–55 images per specimen. Specimens examined included each trunk location in a single old tree, two young trees, three branches (one at each target node), and two roots each from the young and old trees. Because fine pit structures were strongly correlated with D_c and D_b, they were calculated for the other five felled trees after establishing these correlations for each tree location. In each micrograph, we measured D_b, the torus diameter (D_t), the length of the strands (L), the number of strands (N), the thickness of the strands (t_s), and the pore size (D_p) using each pore's mean elliptical diameter within the strands.

Calculation of $\Delta P_{capillary\text{-}seeding}$—We estimated ($\Delta P_{capillary\text{-}seeding}$), which is the pressure difference at which a pit fails as a barrier and allows gas to enter the vascular system. The critical ΔP for air-seeding should be a function of the size of the pores between the strands of the margo (the negative sign expresses a negative pressure, i.e., a tension):

$$\Delta P_{capillary\text{-}seeding} = -4\tau/D_p \quad (1)$$

where τ is the surface tension of water (7.3 $N \cdot cm^{-1}$ at 20°C) (Zimmermann, 1983).

Calculation of $\Delta P_{deflection}$—The ΔP between an embolized tracheid and an adjacent water-filled tracheid acts on the torus and the margo strands. We estimated the $\Delta P_{deflection}$, which is the pressure difference required to cause the pit membrane to deflect all the way to the pit border (as found in pit aspiration) as follows. We first calculated the lateral force (F) exerted across the pit membrane by the ΔP between the water-filled and the embolized tracheids (Petty, 1972; the negative sign expresses a negative pressure, i.e., a tension):

$$F = -0.25\pi D_b^2 \Delta P \quad (2)$$

At any equilibrium displacement of the membrane, this lateral force will be equal to the net restoring force developed during membrane deflection in the radial strands supporting the torus (Bailey and Preston, 1970; Petty, 1972):

$$F = T\sin\theta \quad (3)$$

where T is the tension in each of the strands and θ is their angular displacement. At aspiration, the tension in the strand is a function of the modulus of elasticity (MOE, or ratio between stress and strain) of the strands (taken at 5.0 GPa; Hacke et al., 2004), the strain of the strands (e_{asp}) during stretching and the cross-sectional area of the strands A_s (calculated from t_s, assuming that strands are cylindrical in cross-section):

$$F = \mathrm{MOE} e_{asp} A_s \sin\theta_{max} \quad (4)$$

Assuming that the membrane shape upon stretching followed the border pit curvature, we can replace $\sin\theta_{max}$ by $D_b/2r$, where r is the radius of curvature of the strands at any displacement. It can be shown that $r = d_{max}/2 + D_b^2/(8d_{max})$ and $e_{asp} = (\theta_{asp} r/l - 1)$, where $\theta_{asp} = \arcsin(D_b/2r) - \arcsin(D_t/2r)$. By combining Eqs. 2 and 4 and considering the total number of strands (N) supporting the torus, the pressure difference that corresponds to the maximum deflection of the torus from its normal position to a position touching the pit border is:

$$\Delta P_{deflection} = -2N\,\mathrm{MOE} e_{asp} A_s/(\pi r D_b) \quad (5)$$

Calculation of $\Delta P_{stretch}$—We define another parameter as $\Delta P_{stretch}$, which is the pressure that would be needed to move the membrane on an aspirated pit enough that its torus does not entirely cover the aperture. The edge of the torus (where the strands are attached) is in contact with the edge of the pit aperture, and the torus becomes off-center by being displaced to the right or left. At pressures beyond this value, air seeding can occur through the margo pores exposed at the pit aperture. In this scenario, half of the margo is stretched less than before, but the other half of the margo is stretched more than before, and it

is this second half with which we are concerned. We used the analysis of Sperry and Hacke (2004) and Hacke et al. (2004) that allows membrane deflection beyond aspiration, with the assumption that the torus is inelastic, so all the stretching occurs in the margo. In this case, the restoring force is only applied to the half of the strands that are still under tension. The extra force acting to move the membrane from its maximum deflection at aspiration to the stretching point is then applied to the part of the torus exposed through the aperture and not to the whole membrane (Bolton and Petty, 1978), taken as the surface represented by the average torus and aperture diameters. The pressure difference at membrane stretch is then given by:

$$\Delta P_{\text{stretch}} = \Delta P_{\text{deflection}} - 4N\text{MOE}(e_{\text{stretch}} - e_{\text{asp}})A_s D_b/[\pi r(D_t + D_a)^2] \quad (6)$$

where $(e_{\text{stretch}} - e_{\text{asp}})$ represents the additional strain in the strands when the membrane moves from the aspirated position to the stretched position, with $e_{\text{stretch}} = (\theta_{\text{stretch}} r/l - 1)$, where $\theta_{\text{stretch}} = \arcsin(D_b/2r) - \arcsin(D_a/2r)$.

Calculation of $\Delta P_{rupture}$—Following the analysis of Sperry and Hacke (2004) and Hacke et al. (2004), membrane $\Delta P_{\text{rupture}}$ was reached when the strand stress reached its rupture value, denoted by its tensile strength (taken at 2.2 GPa; Hacke et al., 2004). The extra force acting to move the membrane from its stretching point to its breaking point is then only applied a surface represented by the aperture diameter. At this stage, the stress applied would cause a strand strain of 44%:

$$\Delta P_{\text{rupture}} = \Delta P_{\text{stretch}} - N\text{MOE}(0.44 - e_{\text{stretch}})A_s D_b/(\pi r D_a)^2 \quad (7)$$

Pit and lumen conductivity on a tissue basis—We estimated the specific conductivity of the pits, which represents the parallel conductivity of pits ($k_{\text{s-pit}}$) on a tissue basis (rather than for individual pits) to be able to link P_{50} and the surface represented by pits to pit hydraulic efficiency. Measured whole-wood specific conductivity (k_s) was assumed to represent the conductivities of both lumen and pits together ($k_{\text{s-lumen}}$ and $k_{\text{s-pit}}$, respectively) and as a consequence, $k_{\text{s-pit}}$ was calculated as:

$$k_{\text{s-pit}} = (1/k_s - 1/k_{\text{s-lumen}})^{-1} \quad (8)$$

The root, trunk, and branch xylem k_s's at full saturation (without embolisms) were taken from published data measured on the same samples as the ones used to determine P_{50} (Table 1). Whole-wood $k_{\text{s-lumen}}$ was calculated according to the Hagen–Poiseuille equation for capillaries (Ewers, 1985):

$$k_{\text{s-lumen}} = \frac{T_d \pi \rho \sum_{i=1}^{n} D_i^4}{128\eta n} \quad (9)$$

where ρ is the density of water (kg m^{-3}), η is the dynamic viscosity of water (0.001 Pa · s at 20°C), D is the diameter of the i^{th} tracheid summed over the number of tracheids, n and T_d is the tracheid density or number of tracheids per cross section area (m^{-2}). Tracheid density was estimated by counting the total number of tracheids present in each growth ring divided by the area of the growth ring in each of the hydraulic samples.

Single pit resistance on an area basis—We also estimated the hydraulic resistance of individual pits on an area basis as the sum of twice the aperture area resistance plus the membrane area resistance. Because the average diameters of the pit pores and pit aperture are much smaller than that of the pit chamber, the single pit area resistance was assumed to be largely dependent on the size of the pit aperture and the size and frequency of the margo pores. The resistance of the pit aperture on an area basis was calculated from eqs. 20 and 21 in Sperry and Hacke (2004) using measurements of pit aperture diameter and depth. The membrane area resistance was calculated using eq. 17 in Sperry and Hacke (2004) using the number and diameter of pores as well as the effective fraction of the margo occupied by pores (eq.16 in Sperry and Hacke, 2004). The number of pores in the margo was estimated from the total pore area (margo area minus strand area) divided by the average area of a single pore.

Statistical analysis—Least squares methods were used to fit relationships between the calculated functional parameters for the bordered pit membranes and the various anatomical and hydraulic characteristics. All stated equations had a significant regression coefficient at $P < 0.05$. Differences between old-growth and young trees and among locations (radial and height locations) were determined using a one-way ANOVA. The experiment was designed to assess values at both inner and outer sapwood, but for height location we were interested in an estimate of the entire sapwood. Therefore, the effect of height location was estimated by weighting the values by the proportion of the total sapwood area occupied by the outer and inner sapwood shells (taken from Domec and Gartner, 2001). The inner shell represented the area from the third growth ring exterior to the heartwood–sapwood boundary to the middle of the sapwood zone, and the outer shell represented the area from the middle of the sapwood zone to the cambium. All statistical procedures were conducted with Statistical Analysis Systems software (1999; SAS Inc., Cary, North Carolina, USA).

RESULTS

There were large differences between earlywood and latewood bordered pit morphology for all the characteristics examined in micrographs from SEM (Table 2; Fig. 1A, B) or light microscopy (Table 3), which included bordered-pit diameter (D_b), torus diameter (D_t), pit aperture (D_a), length of the margo strands (L), average pore size with the strands (D_p), strand thickness (t_s), number of margo strands (N), and maximum torus displacement (d_{max}). There were no significant differences between these values for inner vs. outer sapwood,

TABLE 2. Characteristics of bordered pits measured from SEM micrographs of roots, trunks, and branches of young and old Douglas-fir (*Pseudotsuga menziesii*) trees. The node numbers represent the height location in the trunk counting down from the top of the trees. Values at each node in the trunk represent the weighted average between outer and inner sapwood samples. Features are the bordered pit diameter (D_b), torus diameter (D_t), the length of the margo strands (L), the average pore size within the margo (D_p), the thickness of the strands (t_s), and the number of strands (N) supporting the torus in earlywood (EW) and latewood (LW).

	D_b (μm)		D_t (μm)		L (μm)		D_p (μm)		t_s (nm)		N	
Tree location	EW	LW	EW	LW	EW	LW	EW	LW	EW	LW	EW	LW
Root, old	18.4	13.2	7.3	7.1	5.5	3.4	0.54	0.29	79	128	87	114
Root, young	20.4	13.1	8.7	7.8	5.6	3.6	0.65	0.30	72	127	81	120
Trunk base (node 110)	21.5	14.1	9.7	8.2	6.0	2.9	0.61	0.63	158	131	60	62
Trunk node 35	21.1	15.3	9.6	8.5	5.6	3.4	0.47	0.63	155	149	66	65
Trunk node 15	17.5	11.2	8.3	6.4	4.6	2.4	0.35	0.45	111	153	73	67
Trunk node 5	14.8	13.7	6.9	6.4	3.9	3.6	0.37	0.67	128	123	75	53
Trunk, young	17.2	12.3	7.9	5.9	5.7	2.1	0.36	0.57	157	126	65	59
Branch 5	13.9	13.6	6.2	5.7	3.5	3.4	0.37	0.72	136	157	54	49
Branch 15	15.2	12.3	7.4	6.8	3.7	2.7	0.42	0.62	147	134	55	53
Branch 35	14.6	11.8	6.9	6.4	3.8	3.0	0.37	0.58	138	145	55	53
Branch, young	14.9	11.2	7.1	5.9	3.5	2.6	0.38	0.55	157	122	63	54

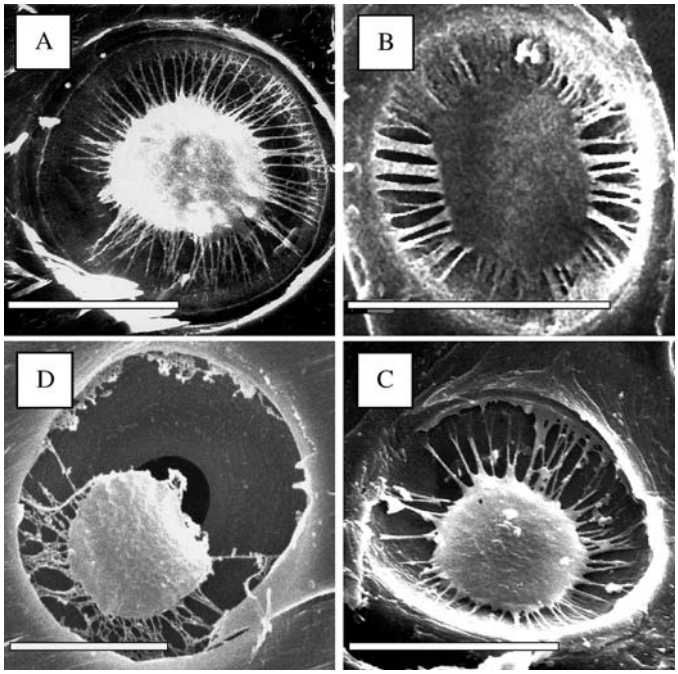

Figure 1. Scanning electron micrographs showing clockwise from upper left (A) a non-aspirated bordered pit in earlywood, (B) a non-aspirated bordered pit in latewood, (C) an aspirated torus in earlywood, and (D) a broken torus in earlywood (after subjecting the sample to an air injection pressure of 5.0 MPa) of *Pseudotsuga menziesii*. Bars represent 10 μm.

so the weighted average is reported for each line in Tables 2 and 3. Pit characteristics varied little either within earlywood or within latewood for a given organ and height, although the pits located near the tracheid tips tended to have lower values than those in the mid-portion (data not shown). There was a moderately strong agreement between D_b measured with the SEM and D_b measured with the light microscope (Tables 2 and 3). A number of the morphological features were autocorrelated. For example, tracheid lumen diameter (D_c) was strongly correlated with earlywood D_b ($r^2 = 0.87$, $D_b = 0.3D_c + 9.4$). When earlywood and latewood data were pooled together, there was also a significant correlation between D_a and D_b ($r^2 = 0.52$, $D_a = 0.32D_b + 0.56$) and between D_t and D_b ($r^2 = 0.70$, $D_t = 0.3D_b + 3.1$).

In latewood, pits had smaller overall diameter (D_b) and a smaller torus and membrane than in earlywood. However, the torus made up a smaller proportion of the membrane in the earlywood than the latewood (45% and 55%, respectively) because torus diameter (D_t) was only 14% smaller in the latewood than earlywood, whereas D_b was almost 30% smaller (Table 2). In earlywood, the strands holding the torus in the roots were about half the thickness (79 nm) of those anywhere else in the tree (Table 2). The average pore diameter (D_p) in earlywood was larger in roots than in branches or trunks (with the exception of the base) for both old trees and young trees (Table 2). In contrast, the latewood D_p was much smaller in roots than in the other locations, with only half the size in many of the comparisons. In the old trees, earlywood D_p was much larger in the roots and near the base of the trunk than in branches.

Next, we used the morphological values and the assumed values for mechanical properties of margo strands to calculate the pressure differences that would cause different types of pit membrane failure. In the presence of embolism, we calculated that the xylem pressure necessary to cause air seeding ($\Delta P_{\text{capillary-seeding}}$) through the margo pores in earlywood ranged from an average of −0.75 MPa in branches to −0.55 MPa in trunks and roots of old trees and to −0.45 MPa in roots of young trees. In earlywood, the calculated pressure required to cause the pit membrane to deflect and potentially aspirate ($\Delta P_{\text{deflection}}$) ranged from an average of −0.02 MPa in roots to −0.47 MPa in branches. In earlywood, the pit membrane deflected and aspirated rather than allowing air seeding through pores in the membrane, as seen by the fact that for any one point, $\Delta P_{\text{deflection}}$ was always higher (less negative) than $\Delta P_{\text{capillary-seeding}}$ (Fig. 2A). Our calculations showed that root pit membranes aspirated at ΔP values much higher (less negative) than stems, which in turn were much higher than branches (Fig. 2A).

In contrast to the earlywood, the latewood pit membranes allowed air seeding rather than pit aspiration, as seen by the fact that for any one point $\Delta P_{\text{deflection}}$ was lower than $\Delta P_{\text{capillary-seeding}}$ (Fig. 2B). In latewood, roots required a

TABLE 3. Characteristics of bordered pits measured from light micrographs of roots, trunks, and branches of young and old Douglas-fir (*Pseudotsuga menziesii*) trees. The node numbers represent the height location on the trunk counting down from the top of the trees. Values at each node in the trunk represent the weighted average between outer and inner sapwood samples. All features are for both earlywood (EW) and latewood (LW): the mean hydraulic diameter (D_c), the bordered pit diameter (D_b), the pit aperture diameter (D_a), the maximum torus displacement (d_{max}), the pit frequency, and the surface represented by pits as a percentage of the radial cell wall area.

		D_b (μm)		D_a (μm)		d_{max} (μm)		Pit frequency (no./mm²)		Surface pits (%)	
Tree location	D_c (μm)	EW	LW	EW	LW	EW	LW	EW	LW	EW	LW
Root, old	37	17.8	14.4	5.9	2.4	0.84	3.30	668	405	20.0	6.2
Root, young	36	18.9	12.2	6.0	2.9	0.87	3.16	551	338	18.3	6.2
Trunk base (node 110)	37	19.4	13.0	7.0	6.9	1.66	4.94	360	224	15.6	7.3
Trunk node 35	32	18.3	14.0	6.7	6.1	1.67	4.06	412	235	17.9	7.1
Trunk node 15	29	17.1	12.6	6.0	5.9	1.60	3.38	505	317	14.8	5.6
Trunk node 5	22	14.1	10.1	5.7	5.0	1.51	2.60	619	375	13.9	7.8
Trunk, young	32	16.9	11.2	6.9	4.0	1.77	2.51	325	237	13.6	4.1
Branch 5	16	13.2	9.9	5.0	3.6	1.52	2.59	612	506	12.7	10.3
Branch 15	17	12.8	10.2	5.0	3.6	1.47	2.43	563	407	13.7	8.8
Branch 35	17	14.1	9.4	5.1	3.5	1.43	2.51	844	518	12.7	8.4
Branch, young	18	13.6	9.8	4.9	3.5	1.46	2.68	518	312	11.9	4.9

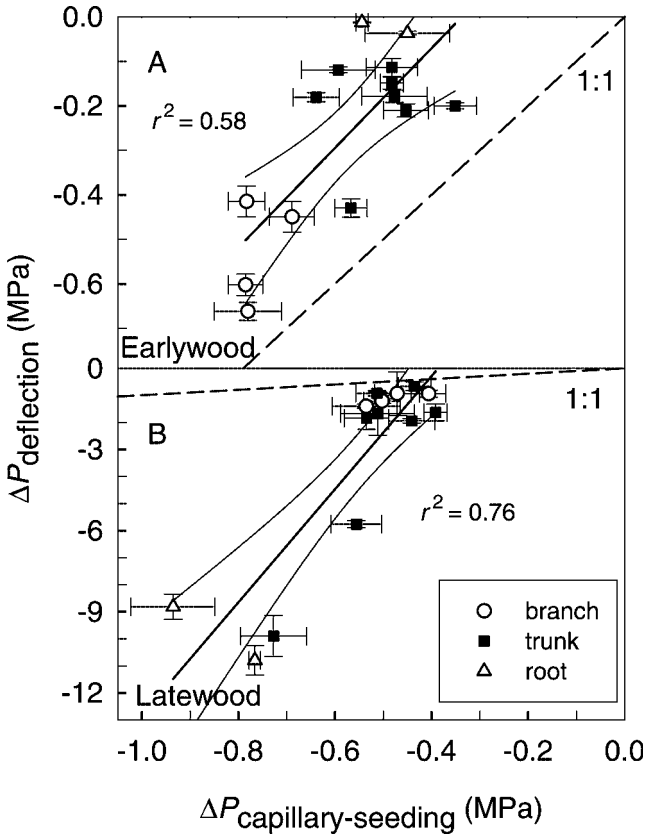

Figure 2. Relationships between the pressure differential required to cause maximum torus deflection ($\Delta P_{deflection}$) and the pressure differential for air to seed through the margo pores ($\Delta P_{capillary\text{-}seeding}$) in (A) earlywood and (B) latewood of *Pseudotsuga menziesii*. Error bars and 95% confidence intervals for the regressions are shown.

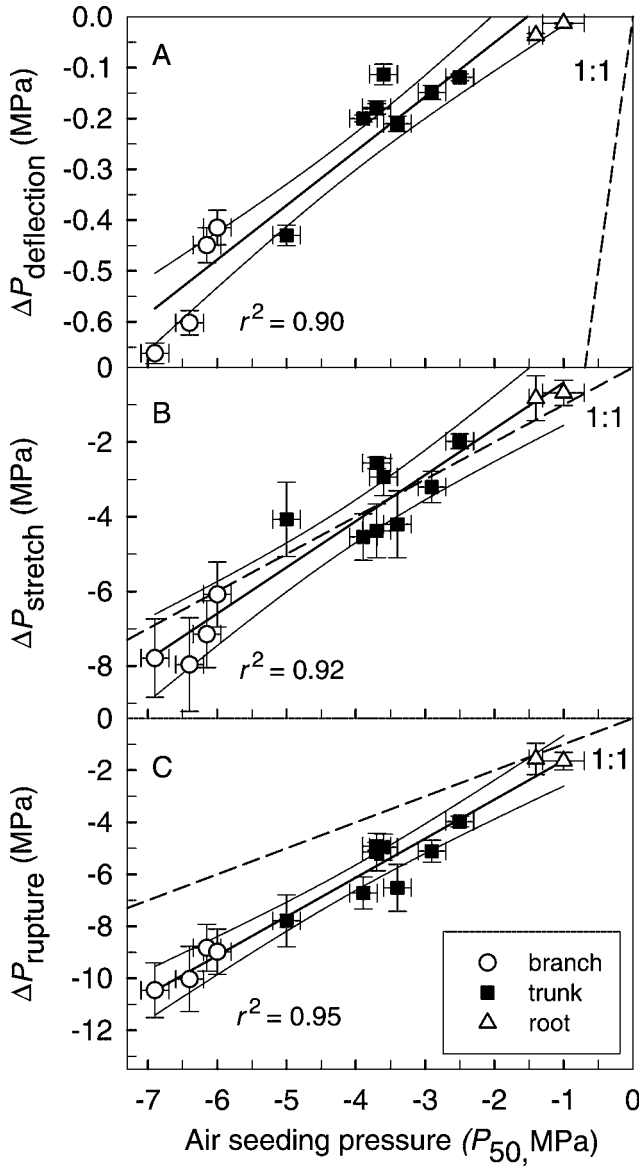

Figure 3. Pressures required (A) to cause maximum torus deflection ($\Delta P_{deflection}$), (B) to stretch the margo ($\Delta P_{stretch}$), and (C) to rupture the margo strands ($\Delta P_{rupture}$) vs. the pressure required to cause 50% loss of conductivity (P_{50}) in earlywood of *Pseudotsuga menziesii*. Error bars and 95% confidence intervals for the regressions are shown.

more negative $\Delta P_{capillary\text{-}seeding}$ than did the rest of the tree to cause the pit to deflect because of the smaller D_p in the roots than in the rest of the tree (Table 2). In the presence of embolism in latewood, the xylem pressures necessary to cause $\Delta P_{capillary\text{-}seeding}$ ranged from −0.5 to −0.9 MPa. These values for branches and trunks from the old trees and roots from the young trees, are pressures experienced in the field (Table 1), suggesting that latewood is often embolized in these locations in the field. For roots of old trees, however, latewood $\Delta P_{capillary\text{-}seeding}$ was more negative than root xylem pressure, and so their latewood tracheids would not embolize.

In the earlywood, the pit membrane will deflect to the maximum extent allowed by the pit border with a relatively small pressure difference ($\Delta P_{deflection}$) compared to the pressure difference required to cause 50% loss of conductivity (P_{50}). The calculated P_{50} derived from vulnerability curves occurred at pressure differences about 1 MPa, 3 MPa, and 6 MPa lower than those differences required for torus deflection for the earlywood in roots, trunkwood, and branches, respectively (Fig. 3A).

The pressure required to stretch the membrane so that the margo is pulled all the way to the edge of the aperture ($\Delta P_{stretch}$) was typically very similar to the pressure required to attain P_{50} for a given sample (Fig. 3B). The slope of the relationship between $\Delta P_{stretch}$ and P_{50} was significantly different from 1 when all data were included ($P = 0.04$, 95% confidence interval on the slope varied between 1.1 and 1.5; Fig. 3B). However, the slope of the relationship did not differ from one when the branch data were excluded ($P = 0.2$; 95% confidence interval on the slope varied between 0.6 and 1.4).

Margo strands ruptured at the least negative pressure difference ($\Delta P_{rupture}$) in roots, followed by trunks and then branches (on average −1.6 MPa in the roots, −5.1 MPa at the tree base and −9.6 MPa in the branches, Fig. 3C). Once the membrane was stretched and P_{50} was reached, there appeared to be an increase in the margin of safety ($\Delta P_{rupture} - \Delta P_{stretch}$) between roots, trunkwood, and branches before pressure was negative enough to rupture the membrane. This margin of safety was on average 2.6 MPa in branches, at the top of the

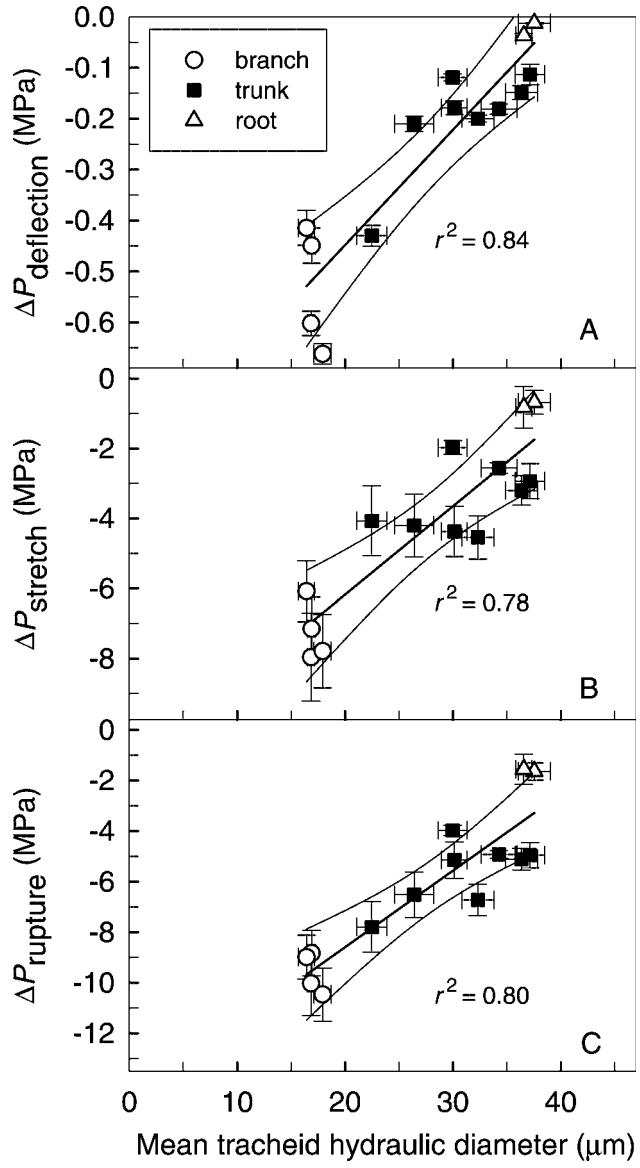

Figure 4. Pressure differentials required (A) to cause maximum torus deflection ($\Delta P_{deflection}$), (B) to stretch the margo strands ($\Delta P_{stretch}$) and (C) to rupture the margo strands ($\Delta P_{rupture}$) in earlywood vs. mean tracheid hydraulic diameter of *Pseudotsuga menziesii*. Error bars and 95% confidence intervals for the regressions are shown.

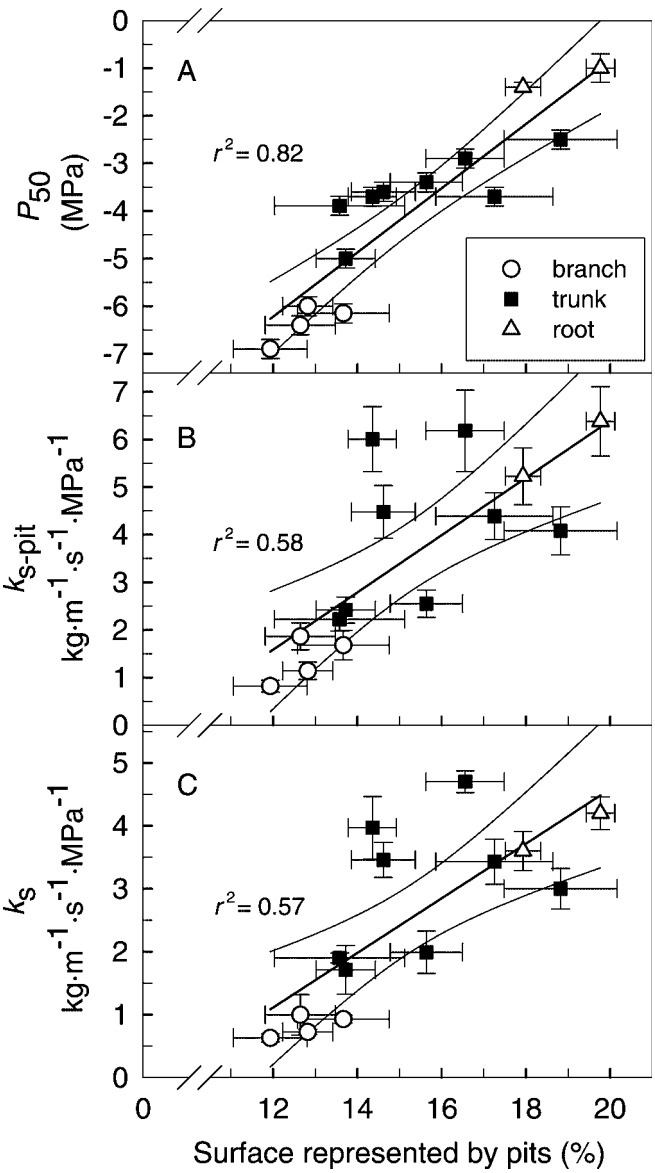

Figure 5. (A) Pressure required to cause 50% loss of conductivity (P_{50}), (B) bordered-pit specific conductivity on a tissue basis ($k_{s\text{-}pit}$) and (C) whole-wood specific conductivity (k_s) vs. the fraction of surface area represented by pits as a percentage of tracheid radial cell wall surface in earlywood of *Pseudotsuga menziesii*. Error bars and 95% confidence intervals for the regressions are shown.

trees and in young trees, 2.0 MPa at the base of the old trees, and only 1.2 MPa and 1.1 MPa in roots from young and old trees, respectively. Outer parts of the sapwood did not have significantly different $\Delta P_{deflection}$, $\Delta P_{stretch}$ or $\Delta P_{rupture}$ than did inner parts ($P = 0.08$, data not shown). The mean hydraulic diameter was lower in trunks and branches than in roots (Table 3) and was positively correlated with $\Delta P_{deflection}$, $\Delta P_{stretch}$, and $\Delta P_{rupture}$ (Fig. 4).

Pit frequency (number of pits/mm^2) of radial tracheid walls was higher in branches than in the trunk ($P < 0.04$, Table 3), and higher in all parts of old trees than young trees ($P < 0.03$). However, in the earlywood, because of the relative pit sizes of different organs (derived from D_b, Table 3), the surface area represented by pits as a percentage of the radial cell wall area tended to be highest in roots followed by trunk and branches (Table 3, Fig. 5). The surface represented by pits in the earlywood was positively correlated with P_{50} (Fig. 5A), bordered-pit specific conductivity ($k_{s\text{-}pit}$, Fig. 5B) and whole-wood specific conductivity (k_s, Fig. 5C).

Average k_s and $k_{s\text{-}pit}$ had a positive linear correlation with vulnerability to embolism (Fig. 6). In the old trees, pits represented as much as 64% of the total xylem resistance to flow in the branches, 81% in the trunks and 66% in the roots. In the young trees, the pit contribution to the total resistance to flow was higher than in the old trees (Table 1).

The single pit resistance on an area basis (pit membrane plus aperture resistances) was mainly due to pit aperture resistance

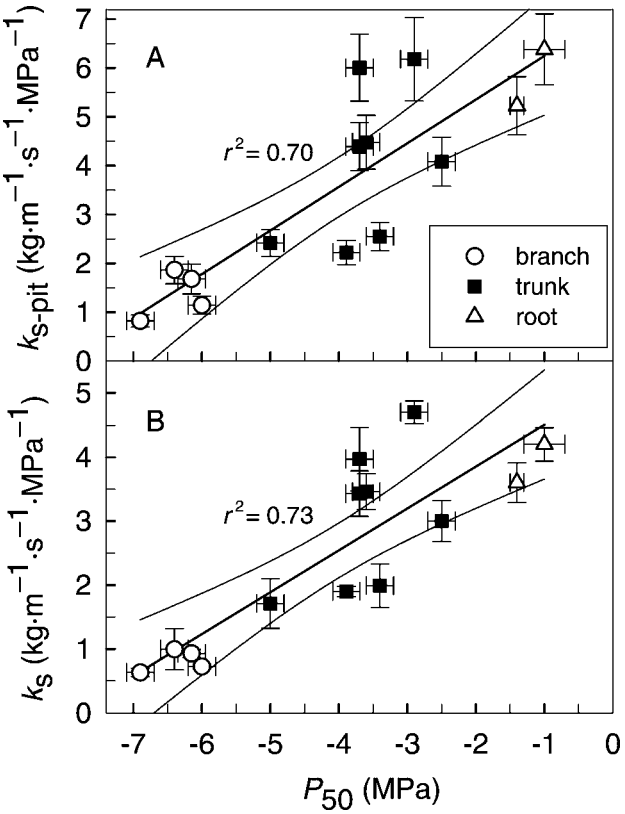

Figure 6. (A) Bordered-pit specific conductivity on a tissue basis ($k_{s\text{-}pit}$) and (B) whole-wood specific conductivity (k_s) vs. the pressure required to cause 50% loss of conductivity (P_{50}) of *Pseudotsuga menziesii*. Error bars and 95% confidence intervals for the regression are shown.

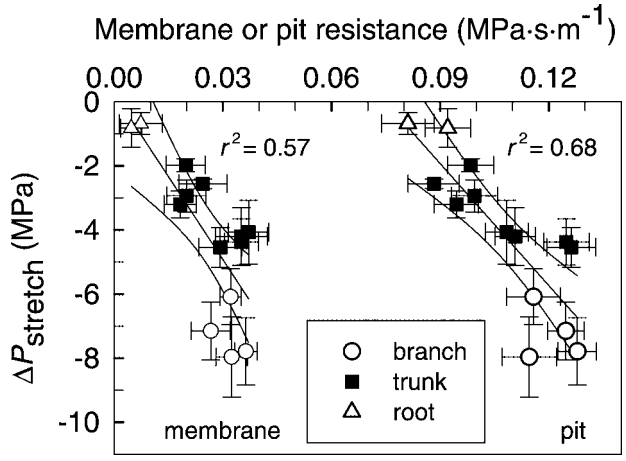

Figure 7. Pressure required to cause stretching of the margo ($\Delta P_{stretch}$) vs. the membrane resistance on area basis (resistance of margo pores) and vs. the single pit resistance on an area basis (membrane plus aperture) in earlywood of *Pseudotsuga menziesii*. The difference between the pit resistance points and the membrane resistance represents the aperture resistance. Error bars and 95% confidence interval for the regression are shown.

on an area basis and increased linearly with both the pit aperture resistance on an area basis and the membrane resistance on an area basis. However, because the intercept of the relationship between single pit resistance and pit membrane resistance (single pit resistance = 1.15 pit membrane resistance + 0.08, $r^2 = 0.61$) was positive and significantly different from zero ($P = 0.04$), the proportion of the single pit resistance represented by membrane resistance increased as membrane resistance increased. Consequently, membrane resistance represented on average 10% of the single pit resistance in the roots, 22% in the trunk and 27% in the branches. The aperture resistance increased with decreasing $\Delta P_{stretch}$ but not significantly ($r^2 = 0.26$, $P = 0.07$), whereas pit membrane resistance and the single pit resistance increased significantly with decreasing $\Delta P_{stretch}$ (Fig. 7). However, the regression lines between $\Delta P_{stretch}$, membrane resistance and single pit resistance were not significantly different from each other ($P = 0.45$, Fig. 7).

There were significant correlations between the minimum xylem pressure sustained at a given location within the tree and margo pore diameters (Fig. 8A), $\Delta P_{stretch}$ (Fig. 8B), and $k_{s\text{-}pit}$ (Fig. 8C). When the regression lines in Figs. 8A and 8C are extrapolated to the *x*-axis, $k_{s\text{-}pit}$ would reach 0 at about −3.0 MPa, which would correspond to a margo pore diameter of 0.24 μm.

In earlywood, there was a significant effect of vertical location on torus diameter and on membrane diameter (Fig. 9A, $P = 0.04$), as well as on margo pore diameter ($P = 0.03$; Fig. 9B). As a consequence, the membrane resistance and the single pit resistance increased significantly with height going from roots to branches ($P = 0.01$; Fig. 9C). Single pit resistance was 25% higher at the trunk base than in the roots, and 30% higher at the top of the trunk than at the base. Branches had similar high single pit area resistance as the top of the trunk.

DISCUSSION

Our results show that the hydraulic safety and efficiency of Douglas-fir xylem were strongly linked to the structural and mechanical properties of tracheid bordered pits. Constraints on relationships between pit structure and function led to a trade-off of efficiency against safety of water transport at both the individual pit and whole wood levels. In addition, spatial variation in bordered pit properties along the plant axis was associated with corresponding variation in xylem conductivity and vulnerability to embolism, which decreased as xylem tension increased from roots to upper branches.

Bordered pit functioning explained the differences in air-seeding thresholds between earlywood and latewood—The main hydraulic functions of earlywood tracheids are to conduct water and to resist high tensions without embolizing. Because the air-seeding pressure ($\Delta P_{capillary\text{-}seeding}$) was lower (more negative) than pressure required to deflect the membrane ($\Delta P_{deflection}$), embolism developing in earlywood tracheids would not spread to adjacent tracheids through the margo pores. This study revealed quantitatively what has been inferred qualitatively (Sperry and Tyree, 1990), that the pressure differential required for earlywood membrane stretching was similar to the resistance to embolism (P_{50}), suggesting that the actual mode of air seeding is by elastic stretching of the membrane rather than by the breakage of the membrane (rupture seeding). Stretching to the edge of the pit aperture would create an air-water interface and embolism would spread. Even a narrow gap of 0.05 μm in diameter between the

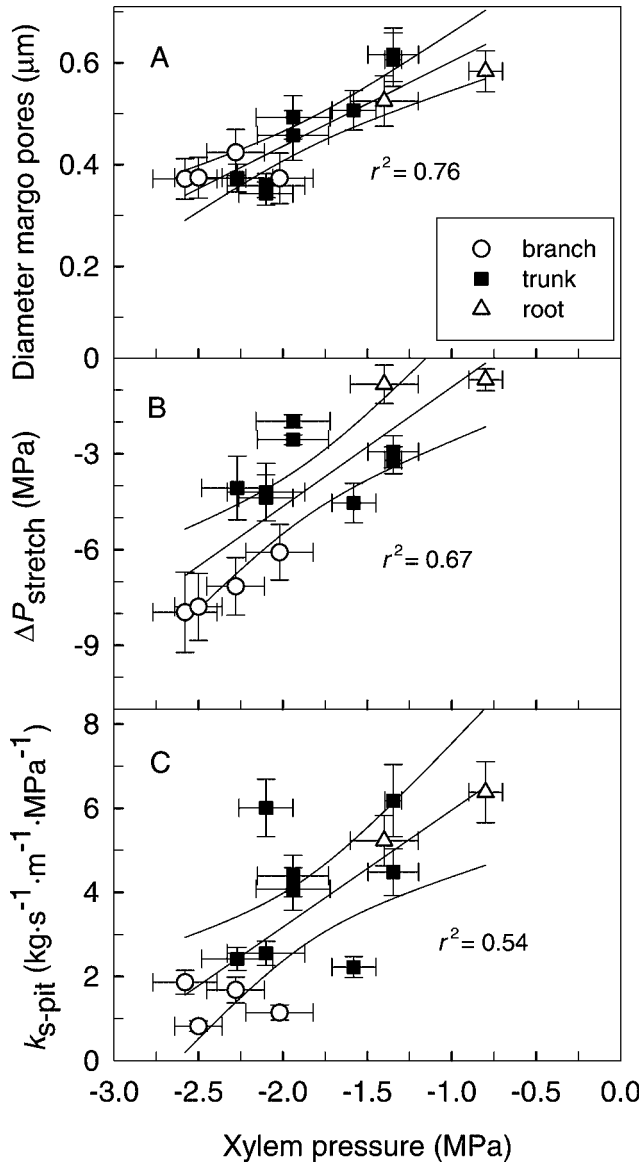

Figure 8. (A) Bordered-pit specific conductivity on a tissue basis ($k_{s\text{-}pit}$), (B) pressure required to cause stretching of the margo ($\Delta P_{stretch}$), and (C) margo pore diameter in earlywood vs. minimum xylem pressure (water potential) of *Pseudotsuga menziesii*. Error bars and 95% confidence intervals for the regressions are shown.

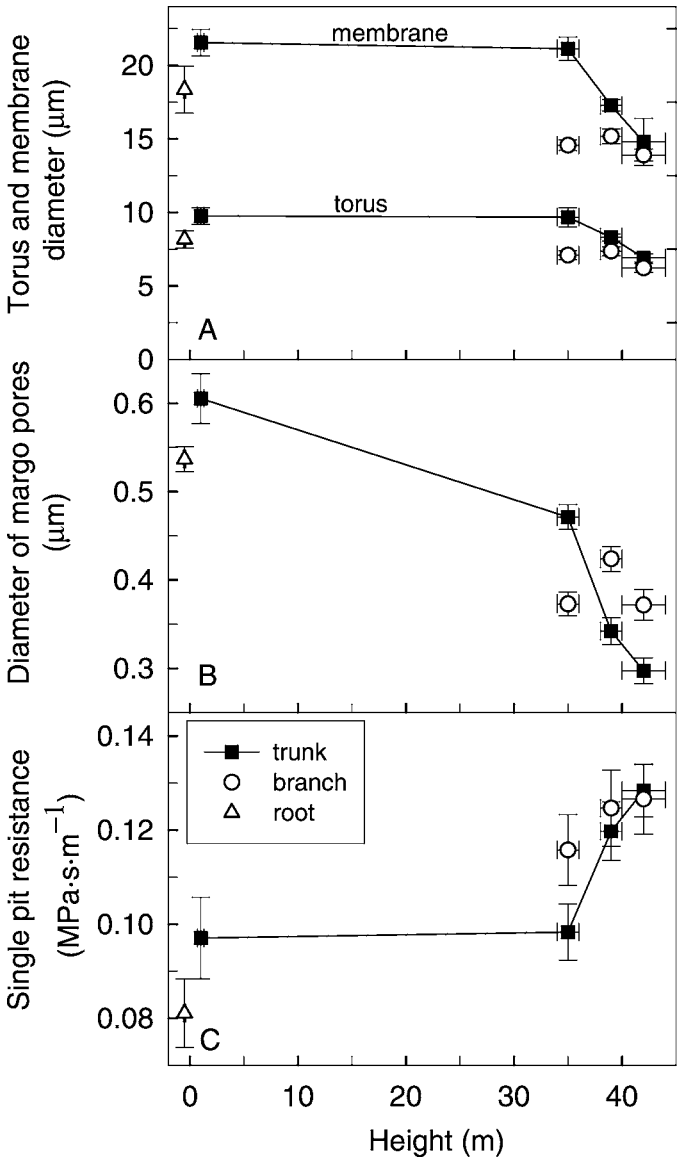

Figure 9. (A) Torus and bordered pit membrane diameters, (B) margo pore diameter, and (C) single pit resistance on an area basis in earlywood vs. heights in old trees of *Pseudotsuga menziesii*.

torus and the bordered pit aperture cannot withstand more than −6 MPa before air enters.

The low resistance to embolism of latewood inferred from cryo-SEM images (Utsumi et al., 2003) or determined from vulnerability curves and measured water content (Domec and Gartner, 2002b) was also explained by the properties of its bordered pit membranes. The small torus and the thick margo strands in latewood prevented the torus from slipping from its sealed position and did not allow the margo to prevent air bubbles from spreading from one embolized tracheid to another. However, these studies also showed that at lower negative pressures, some of the latewood tracheids would embolize to a lesser extent than would earlywood and more than 40% of the latewood conductivity would remain (Domec and Gartner, 2002b), probably because the smallest latewood tracheids also bear the smallest margo pores. This result may explain why, when using the staining method, Sperry and Tyree (1990) showed that latewood of three conifer species continued to be conductive after earlywood tracheids had embolized. Within the latewood section of the growth ring, we can expect that the first few latewood tracheids represent its major conductive part. The 40% of the latewood conductivity remaining at low negative pressures would then be due to the majority of the small latewood tracheids that are still functional, giving the impression when using dye that most of the latewood is still conductive.

Bordered pit resistivity not lumen resistivity determined water transport efficiency—The fraction of the tracheid radial wall surface occupied by pits was a good predictor of the

bordered-pit specific conductivity on a tissue basis ($k_{s\text{-}pit}$), consistent with modeling results about the effect of pit size and number on the overall resistance to water flow (Lancashire and Ennos, 2001; Hacke et al., 2004). Because the average diameters of the pit aperture and of the pit pores are much smaller than that of the tracheid lumens, bordered pits represented as much as 50% and 70% of the overall resistance to water flow in branches and roots, respectively (Table 1). This is in agreement with previous modeling and experimental work done on pit resistivity in conifers (Schulte and Gibson, 1988; Lancashire and Ennos, 2002). Lumen and pit resistivities in narrow tracheids of branches were almost co-limiting, which also was in agreement with a modeling study of pit resistance in conifers (Hacke et al., 2004). Although the lumen resistivity was not negligible, it did not vary in proportion to the total resistivity as pit resistivity did (Valli et al., 2002). The decreasing hydraulic diameter from roots to branches was also highly correlated with bordered pit functioning, indicating that basic anatomical properties are robust predictors of water transport properties (Fig. 4).

Trade-off of hydraulic conductivity against resistance to embolism is determined by bordered pit structure—Plants must maintain a delicate balance between maximizing water transport and limiting the risk of embolism and loss of hydraulic conductance. In the present study, resistance to embolism (lower P_{50}) increased at the cost of a decrease in k_s mainly through a reduction in $k_{s\text{-}pit}$ (Fig. 6). At the tissue level, a trade-off of water transport efficiency against resistance to water-stress-induced embolism has been hypothesized (Tyree and Ewers, 1991). Although this trade-off is more difficult to detect across individual Douglas-fir trees (Kavanagh et al., 1999), it has been observed within an individual (Domec and Gartner, 2001).

Perhaps the empirical relationship between the percentage of radial surface that is covered with pits and P_{50} can be explained by the strong correlation between wall implosion resistance and P_{50} (Hacke et al., 2004). A low P_{50} set by individual pit structure and functioning means greater negative pressures, which requires a stronger wall to avoid wall collapse, which in turn requires a smaller pitted fraction of the cell wall. In angiosperms, the total pit area per conduit also scaled with embolism resistance (Hacke et al., 2006), but it may be related to the random occurrence of large pores in pit membranes rather than the fraction of pit area per se. Plants may not have perfect control over the pore size in homogenous pit membranes (Choat et al., 2003), and the more pits there are in a vessel, the greater is the likelihood that a vessel has large pores (Choat et al., 2004; Wheeler et al., 2005).

At the individual pit level, the existence of a trade-off between an efficient and a safe bordered pit was supported by the strong correlation between single pit resistance (more resistance means lower conductivity and less transport efficiency) and $\Delta P_{stretch}$ (more negative values mean that greater pressure differentials can be sustained before critical stretching and air seeding occur) (Fig. 7). In trunks, Douglas-fir made pits with increasing safety and decreasing specific conductivity with height. This pattern resulted from having smaller pits, a smaller percentage of the tracheid wall area that is covered with pits, smaller pit aperture, and less porous membranes (from having smaller pores within the pit membranes) with height. In contrast, roots had low single pit resistance (membrane resistance plus aperture resistance), but had pits that would air seed at less negative pressures than did the trunks. Last, branches had smaller bordered pits that sealed more effectively but also constrained pit conductivity because they were made of less conductive pit apertures and pores in the margo.

Trunk segmentation in relation to bordered pit functioning with height—For the last decade, research on determinants of maximum tree height has focused on hydraulic limitations associated with path length (Ryan and Yoder, 1997) and on gravitational or hydrostatic constraints (Koch et al., 2004; Woodruff et al., 2004). However, our results suggest that pit membrane structure may play a role in limiting maximum tree height. At the top of trees, the pit membrane is required to have small pores to avoid embolism, but with such small pores, specific conductivity is limited. For example, an extrapolation of the regression line in Fig. 8C shows that $k_{s\text{-}pit}$ becomes zero at a xylem pressure of about −3 MPa, which is about 0.5 MPa lower than the minimum xylem pressure measured in a 65-m-tall Douglas-fir (Bauerle et al., 1999).

Bordered pits in earlywood will deflect, stretch, and rupture at more negative pressures in the branches and at the top of the trees than at the bottom and in the roots. The pit sizes and therefore $k_{s\text{-}pit}$ and k_s tended to be smaller at the top and in the branches than at the base of the trunk and in the roots. The membrane had lower resistance but was more flexible and withstood higher negative pressures before stretching and breaking in the roots and at the base than at the top of the tree (Fig. 9). Roots have higher k_s and are generally more vulnerable to water-stress-induced embolism than stems and branches (Choat et al., 2005), and thus we predict that intraspecific variations in pore diameter and membrane flexibility also have adaptive consequences for water transport and resistance to drought, respectively. Although the air-seeding pressure was not directly constrained by the pore size, smaller pores also meant thicker strands and therefore higher pressure required to stretch the membrane (Fig. 7). Pit structures were coordinated with the size of the bubble that could be held at the interface of an embolized and a water-filled tracheid. Based on the capillary-seeding equation (Eq. 1) and the trend in xylem pressure from the roots to the upper branches, we can infer that the margo pore diameters should become progressively smaller from roots to terminal branches in order to ensure that the radii of bubbles at air-water interfaces remain small enough to allow the surface tension of water to prevent the spread of embolism (Figs. 8, 9B). The negative pressure adjacent to the cambium at the time of xylem differentiation could act as a signal on tracheid initials during cell wall formation to modify cell wall and bordered pit structure with height or location.

Methodological issues—There are measurement uncertainties in the modulus of elasticity (MOE) and rupture of margo strands that directly affect estimates of $\Delta P_{stretch}$. Direct measurements of microfibril MOE vary from 5–9 GPa (Hepworth and Vincent, 1998; Hancock et al., 2000; Eichhorn and Young, 2001). For the membrane stretching to be within 10% of the P_{50} values, we should have used a lower MOE for the branches and in the trunkwood at the top of the trees (estimated at 3.5 GPa instead of 5.0 GPa) and a higher MOE in the roots (6.0 GPa). One experiment showed that the MOE of cell wall is lower in branches than in trunkwood because of a higher lignin content in the branches (Reiterer et al., 1999). The

cell walls contain varying amounts of cellulose, hemicellulose, and lignin, and the angle of the cellulose microfibrils also varies among cell types and with location. It is thought that pit membranes are relatively close in composition to the compound middle lamella, and as such, may contain a relatively high proportion of lignin (Gindl et al., 2001). Bergander and Salmén (2002) summarized values for the longitudinal MOE of wood cell wall components to be 2.0 GPa for lignin, 7.0 GPa for hemicellulose, and 167.5 GPa for cellulose. Therefore, if a small amount of cellulose is added then the membrane flexibility will change significantly and may influence repeated embolism and refilling cycles.

Additional stress beyond the elastic limit of the strands will result in permanent deformation (as rupture is approached) and removal of the stress will only result in a partial recovery of the strain. With the strand elastic values used in this study, the strain at full aspiration was less than 1% in the roots and trunk and around 2% in the branches. At stretch, the strain in the strands varied between 18% in the trunk to 30% in roots and branches. If we consider that irreversible stretching takes place at a strain of 10–15% (Veytsman and Cosgrove, 1998), creep and irreversible membrane damage are more likely to occur in the roots and branches than in the trunk. Strains during stretching beyond the elastic limit are likely to weaken the chemical bonding of the membrane because it seems impossible that plants could repair their cellulose microfibrils within their dead tracheid cells. Even though conifers appear to go through embolism and refilling cycles under laboratory and field conditions (Edwards et al., 1994; Mayr et al., 2002; Domec et al., 2005), this elastic functioning of the membrane can explain the phenomenon of embolism fatigue (Hacke et al., 2001). Although bordered pit membranes deteriorated with age in one hardwood species (Sperry et al., 1991), our results suggest that between outer and inner sapwood at the base of the trunk of this coniferous species, pit membrane functioning was sustained for more than 35 years. If actual rupture of the membrane had occurred in older inner sapwood samples, the weakening effect would be permanent and P_{50} would be much less negative and would not match the $\Delta P_{stretch}$ calculated.

The fine structural features of bordered pit membranes are important for both tree hydraulic function in vivo and pressure treatment of wood (Singh et al., 1999). The values measured for the various bordered pit features using SEM were in agreement with those published elsewhere (Liese and Bauch, 1967; Fengel, 1972). Our results showed greater strand thicknesses than the single value of 30 nm first used but not measured directly by Petty (1972) and later used to model bordered pit functioning (Bolton and Petty, 1978; Hacke et al., 2004). However, if one looks directly (Petty and Preston, 1969; Petty, 1972) or indirectly by measuring the strand thickness on published images (Jutte and Spit, 1968; Bauch et al., 1972; Singh et al., 1999), one finds that the average thickness in various conifers is between 70 and 140 nm, very close to the average values measured in this study (Table 2).

Recent studies have shown that in angiosperms, modeled values of pit membrane resistance (Sperry and Hacke, 2004) can differ significantly from measured values (Wheeler et al., 2005). In our study, the fact that modeled values were based on anatomical observations represents an improvement over previous approaches. Although the membrane resistance and aperture resistance scale with the third power of pore diameter, we can expect that even if the measured pit characteristics were shifted a little, the trends and relationships presented in this study would be the same. Finally, although good correlation between membrane porosity and vulnerability to embolism has shown using polystyrene microspheres (Jarbeau et al., 1995), recent experiments with colloidal gold did not reveal pores in the expected size range and have indicated that pit membrane pores in angiosperm species were smaller than expected based on air-seeding thresholds (Shane et al., 2000; Choat et al., 2003). In conifers, and probably because pores are an order of magnitude larger than in angiosperms, images taken with SEM techniques are likely to be accurate (Thomas and Nicholas, 1966; Jansen et al., 1998). In an ongoing study on conifer species with a distinct torus and margo (J.-C. Domec, unpublished data), we found a good agreement between margo pore sizes estimated from SEM and estimated using gold colloids.

LITERATURE CITED

BAILEY, P., AND R. PRESTON. 1970. Some aspects of softwood permeability. *Holzforschung* 24: 37–45.

BAUCH, J. W., W. LIESE, AND R. SCHULTZE. 1972. The morphological variability of the bordered pit membranes in gymnosperms. *Wood Science and Technology* 6: 165–165.

BAUERLE, W. L., T. M. HINCKLEY, J. CERMAK, J. KUCERA, AND K. BIBLE. 1999. The canopy water relations of old-growth Douglas-fir trees. *Trees* 13: 211–217.

BEGG, J. E., AND N. C. TURNER. 1970. Water potential gradients in frilled tobacco. *Plant Physiology* 46: 343–345.

BERGANDER, A., AND L. SALMÉN. 2002. Cell wall properties and their effects on the mechanical properties of fibers. *Journal of Material Science* 37: 151–156.

BOLTON, A. J., AND J. A. PETTY. 1978. A model describing axial flow of liquids through conifer wood. *Wood Science and Technology* 12: 37–48.

CHOAT, B., M. BALL, J. LULY, AND J. HOLTUM. 2003. Pit membrane porosity and water stress-induced cavitation in four co-existing dry rainforest tree species. *Plant Physiology* 131: 41–48.

CHOAT, B., S. JANSEN, M. A. ZWIENIECKI, E. SMETS, AND N. M. HOLBROOK. 2004. Changes in pit membrane porosity due to deflection and stretching: the role of vestured pits. *Journal of Experimental Botany* 55: 1569–1575.

CHOAT, B., E. C. LAHR, P. J. MELCHER, M. A. ZWIENIECKI, AND N. M. HOLBROOK. 2005. The spatial pattern of air seeding thresholds in mature sugar maple trees. *Plant, Cell and Environment* 28: 1094–1102.

COCHARD, H., P. CRUIZIAT, AND M. T. TYREE. 1992. Use of positive pressures to establish vulnerability curves. *Plant Physiology* 100: 205–209.

CROMBIE, D. S., M. F. HIPKINS, AND J. A. MILBURN. 1985. Gas penetration of pit membranes in the xylem of *Rhododendron* as the cause of acoustic detectable sap cavitation. *Australian Journal of Plant Physiology* 12: 445–453.

DIXON, M. A., AND M. T. TYREE. 1984. A new hygrometer, corrected for temperature gradients and calibrated against the pressure bomb. *Plant, Cell and Environment* 7: 693–697.

DOMEC, J.-C., AND B. L. GARTNER. 2001. Cavitation and water storage in bole segments of mature and young Douglas-fir trees. *Trees* 15: 204–214.

DOMEC, J.-C., AND B. L. GARTNER. 2002a. Age and position-related in hydraulic vs. mechanical dysfunction of xylem: inferring the design criteria for Douglas-fir wood structure. *Tree Physiology* 22: 91–104.

DOMEC, J.-C., AND B. L. GARTNER. 2002b. How do water transport and water storage differ in coniferous earlywood and latewood? *Journal of Experimental Botany* 53: 2369–2379.

DOMEC, J.-C., F. C. MEINZER, B. L. GARTNER, AND D. R. WOODRUFF. 2006. Transpiration induced axial and radial tensions in Douglas-fir trees. *Tree Physiology* 26: 275–284.

DOMEC, J.-C., M. L. PRUYN, AND B. L. GARTNER. 2005. Axial and radial

profiles in conductivities, water storage and native embolism in trunks of young and old-growth ponderosa pine trees. *Plant, Cell and Environment* 28: 1103–1113.

DOMEC, J.-C., J. M. WARREN, F. C. MEINZER, J. R. BROOKS, AND R. COULOMBE. 2004. Native root xylem embolism and stomatal closure in stands of Douglas-fir and ponderosa pine: mitigation by hydraulic redistribution. *Oecologia* 141: 7–16.

EDWARDS, W. R. N., P. G. JARVIS, J. GRACE, AND J. B. MONCRIEFF. 1994. Reversing cavitation in tracheids of *Pinus sylvestris* L. under negative water potential. *Plant, Cell and Environment* 17: 389–397.

EICHHORN, S. J., AND R. J. YOUNG. 2001. The Young's modulus of microcrystalline cellulose. *Cellulose* 8: 197–207.

EWERS, F. W. 1985. Xylem structure and water conduction in conifer trees, dicot trees and lianas. *International Association of Wood Anatomists Bulletin* 6: 309–317.

EXLEY, R. R., B. G. BUTTERFIELD, AND B. A. MEYLAN. 1973. Preparation of wood specimens for the scanning electron microscope. *Journal of Microscopy* 101: 21–30.

FENGEL, D. 1972. Structure and function of the membrane in softwood bordered pits. *Holzforschung* 26: 3–9.

FUJII, T., S. J. LEE, N. KURODA, AND Y. SUZUKI. 2001. Conductive function of intervessel pits through a growth ring boundary of *Machilus hunbergii*. *International Association of Wood Anatomists Journal* 22: 1–14.

GINDL, W., H. S. GUPTA, AND C. GRÜNWALD. 2001. Lignification of spruce tracheid secondary cell walls related to longitudinal hardness and modulus of elasticity using nano-indentation. *Canadian Journal of Botany* 80: 1029–1033.

HACKE, U. G., J. S. SPERRY, AND J. PITTERMANN. 2004. Analysis of circular bordered pit function. II. Gymnosperm tracheids with torus-margo pit membranes. *American Journal of Botany* 91: 386–400.

HACKE, U. G., J. S. SPERRY, J. K. WHEELER, AND L. CASTRO. 2006. Scaling of angiosperm xylem structure with safety and efficiency. *Tree Physiology* 26: 689–701.

HACKE, U. G., V. STILLER, J. S. SPERRY, J. PITTERMANN, AND K. A. MCCULLOH. 2001. Cavitation fatigue: embolism and refilling cycles can weaken cavitation resistance of xylem. *Plant Physiology* 125: 779–779.

HANCOCK, B. C., S. D. CLAS, AND K. CHRISTENSEN. 2000. Micro-scale measurement of the mechanical properties of compressed pharmaceutical powders. 1. The elasticity and fracture behavior of microcrystalline cellulose. *International Journal of Pharmacy* 209: 27–35.

HEPWORTH, D. G., AND J. F. V. VINCENT. 1998. Modelling the mechanical properties of xylem tissue from tobacco plants (*Nicotiana tabacum* 'Samsun'). *Annals of Botany* 81: 761–770.

JANSEN, S., P. BAAS, P. GASSON, F. LENS, AND E. SMETS. 2004. Variation in xylem structure from tropics to tundra: evidence from vestured pits. *Procceedings of the National Academy of Sciences, USA* 101: 8833–8837.

JANSEN, S., P. KITIN, H. DE PAUW, M. IDRIS, H. BEECKMAN, AND E. SMETS. 1998. Preparation of wood specimens for transmitted light microscopy and scanning electron microscopy. *Belgium Journal of Botany* 131: 41–49.

JARBEAU, J. A., F. W. EWERS, AND S. D. DAVIS. 1995. The mechanism of water stress induced embolism in two species of chaparral shrubs. *Plant, Cell and Environment* 18: 189–196.

JUTTE, S. M., AND B. J. SPIT. 1968. The submicroscopic structure of bordered pits on the radial walls of tracheids in Panama one, Kauri and European spruce. *Holzforschung* 22: 68–175.

KAVANAGH, K. L., B. J. BOND, S. N. AITKEN, B. L. GARTNER, AND S. KNOWE. 1999. Shoot and root vulnerability to xylem cavitation in four populations of Douglas-fir seedlings. *Tree Physiology* 19: 31–37.

KITIN, P. B., T. FUJII, H. ABE, AND R. FUNADA. 2004. Anatomy of the vessel network within and between tree rings of *Fraxinus lanuginosa* (Oleaceae). *American Journal of Botany* 91: 779–788.

KOCH, G. W., S. C. SILLETT, G. M. JENNINGS, AND S. D. DAVIS. 2004. The limits to tree height. *Nature* 428: 851–854.

KOLB, K. J., AND J. S. SPERRY. 1999. Transport constraints on water use by the Great Basin shrub, *Artemisia tridentata*. *Plant, Cell and Environment* 22: 925–925.

KONRAD, W., AND A. ROTH-NEBELSICK. 2005. The significance of pit shape for hydraulic isolation of embolized conduits of vascular plants during novel refilling. *Journal of Biological Physics* 31: 57–71.

LANCASHIRE, J. R., AND A. R. ENNOS. 2002. Modelling the hydrodynamic resistance of bordered pits. *Journal of Experimental Botany* 53: 1485–1485.

LEWIS, A. M. 1988. A test of the air seeding hypothesis using *Sphagnum* halocysts. *Plant Physiology* 87: 577–582.

LIESE, W., AND J. BAUCH. 1967. On the closure of bordered pits in conifers. *Wood Science and Technology* 1: 1–13.

MAHERALI, H., W. T. POCKMAN, AND R. B. JACKSON. 2004. Adaptive variation in the vulnerability of woody plants to xylem cavitation. *Ecology* 85: 2184–2199.

MAYR, S., M. WOLFSCHWENGER, AND H. BAUER. 2002. Winter-drought induced embolism in Norway spruce (*Picea abies*) at the alpine timberline. *Physiologia Plantarum* 115: 74–80.

MCCULLY, M. E, AND M. J. CANNY. 1988. Pathways and processes of water and nutrient movement in roots. *Plant and Soil* 111: 159–170.

PETTY, J. A. 1972. The aspiration of bordered pits in conifer wood. *Proceedings of the Royal Society of London, B, Biological Sciences* 181: 395–395.

PETTY, J. A., AND R. D. PRESTON. 1969. The dimensions and number of pit membrane pores in conifer wood. *Proceedings of the Royal Society of London, B, Biological Sciences* 172: 137–151.

PETTY, J. A., AND G. S. PURITCH. 1970. The effects of drying on the structure and permeability of the wood *Abies grandis*. *Wood Science and Technology* 4: 140–154.

RASBAND, W. 1996. NIH Image. [computer program] National Institutes of Health, Bethesda, Maryland, USA.

REITERER, A., H. LICHTENEGGER, S. TSCHEGG, AND P. FRATZL. 1999. Experimental evidence for a mechanical function of the cellulose microfibril angle in wood cell walls. *Philosophical Magazine A* 79: 2173–2184.

RYAN, M. G., AND B. J. YODER. 1997. Hydraulic limits to tree height and tree growth. *BioScience* 47: 235–242.

SCHULTE, P. J., AND A. C. GIBSON. 1988. Hydraulic conductance and tracheid anatomy in six species of extant seed plants. *Canadian Journal of Botany* 66: 1073–1079.

SHANE, M. W., M. E. MCCULLY, AND M. J. CANNY. 2000. Architecture of branch-root junctions in maize: structure of the connecting xylem and porosity of pit membranes. *Annals of Botany* 85: 613–624.

SINGH, A., B. DAWSON, R. FRANICH, F. COWAN, AND J. WARNES. 1999. The relationship between pit membrane ultrastructure and chemical impregnability of wood. *Horlforshung* 53: 341–346.

SPERRY, J. S., AND U. G. HACKE. 2004. Analysis of circular bordered pit function. I. Angiosperm vessels with homogenous pit membranes. *American Journal of Botany* 91: 369–385.

SPERRY, J. S., A. H. PERRY, AND J. E. M. SULLIVAN. 1991. Pit membrane degradation and air-embolism formation in aging xylem vessels of *Populus tremuloides* Michx. *Journal of Experimental Botany* 42: 1399–1406.

SPERRY, J. S., AND M. T. TYREE. 1990. Water-stress-induced xylem embolism in three species of conifers. *Plant, Cell and Environment* 13: 427–436.

STONE, C. D. 1939. A study on the bordered pits of Douglas-fir with reference to the permeability of wood to liquids. M.S. thesis, Oregon State University, Corvallis, Oregon, USA.

THOMAS, R. J., AND D. D. NICHOLAS. 1966. Pit membrane structure in loblolly pine as influenced by solvent exchange drying. *Forest Product Journal* 16: 53–56.

TYREE, M. T., S. D. DAVIS, AND H. COCHARD. 1994. Biophysical perspectives of xylem evolution: is there a tradeoff of hydraulic efficiency for vulnerability to dysfunction? *International Association of Wood Anatomists Journal* 15: 335–360.

TYREE, M. T., AND F. W. EWERS. 1991. The hydraulic architecture of trees and other woody plants. *New Phytologist* 119: 345–360.

UTSUMI, Y., Y. SANO, R. FUNADA, J. OHTANI, AND S. FUJIKAWA. 2003. Seasonal

and perennial changes in the distribution of water in the sapwood of conifers in a sub-frigid zone. *Plant Physiology* 131: 1826–1833.

VALLI, A., A. KOPONEN, T. VESALA, AND J. TIMONEN. 2002. Simulation of water flow through bordered pits of conifer xylem. *Journal of Statistical Physics* 107: 121–142.

VEYTSMAN, B. A., AND D. J. COSGROVE. 1998. A model of cell wall expansion based on thermodynamics of polymer networks. *Biophysical Journal* 75: 2240–2250.

WHEELER, J. K., J. S. SPERRY, U. HACKE, AND N. HOANG. 2005. Inter-vessel pitting and cavitation in woody Rosaceae and other vesselled plants. *Plant, Cell and Environment* 28: 800–812.

WOODRUFF, D R., B. J. BOND, AND F. C. MEINZER. 2004. Does turgor limit growth in tall trees? Plant, Cell and Environment 27: 229–236.

ZIMMERMANN, M. H. 1983. Xylem structure and the ascent of sap. Springer-Verlag, Berlin, Germany.